Available online at www.sciencedirect.com

SCIENCE DIRECT®

Tectonophysics 388 (2004) 213–224

TECTONOPHYSICS

www.elsevier.com/locate/tecto

The effects of out-of-plane seismic energy on reflections in crustal-scale 2D seismic sections

B.J. Drummond[a,*], R.W. Hobbs[b], B.R. Goleby[a]

[a]*Geoscience Australia, GPO Box 378, Canberra ACT 2601, Australia*
[b]*Bullard Laboratories, Cambridge University, Madingley Road, Cambridge CB3 0EZ, UK*

Received 5 August 2003; received in revised form 15 January 2004; accepted 13 June 2004
Available online 26 August 2004

Abstract

Crustal-scale seismic surveys mostly collect data along single profiles, and the data processing has an underlying assumption that the data have imaged two-dimension (2D) structure striking at right angles to the seismic profile. However, even small amounts of out-of-plane topography on a reflector can result in reflections that do not map the reflector shape accurately. Out-of-plane energy will migrate within the plane of the section to an apparent depth (represented as two-way-time, TWT) that is greater than the depth of the reflection point out of the plane of the section. It will fall within the plane of the section at depths less than, equal to or greater than the intersection of the reflector with the plane of the section, depending on both the amount of out-of-plane topographic relief on the reflector, and the offset of the topographic relief from the plane of the section. Reflectors that are a single surface can therefore be manifested in the seismic section as a band of several reflections, rather than a single reflection. More complex reflectors, such as shear zones that have a finite thickness because they are made up of several to many anastomosing layers of altered and anisotropic rock embedded in protolith, will appear as laterally short reflections within a laterally continuous reflection band. Other examples of such reflectors would be the Moho in some places, and rock with compositional layering. With increasing out-of-plane topographic relief on the reflector, the top of the reflection band for both single- and multi-layer reflectors will be a poor indicator of the top of the reflector in the Earth. The bottom of the reflection band will always be a poor indicator of the bottom of the reflector. Because out-of-plane energy can arrive at TWTs that are different from those of the reflector in the plane of the section, out-of-plane energy has the potential to interfere constructively or destructively with the in-plane energy. In synthetic data calculated for a simple model assuming one layer and topographic relief of 250 m over wavelengths of 4–5 km, similar to that imaged in a real sub-horizontal detachment, amplitudes ranged up to 2.6 times the expected amplitude for the layer. A model with anastomosing layers built to resemble a thick shear zone rather than a discrete fault surface allowed tuning between layers. The effects of out-of-plane energy when combined with the effects of tuning caused amplitudes up to 3.1 times those expected. Larger amplitudes could be achieved if a suitable model was contrived. The results indicate that care must be taken when calculating impedance

* Corresponding author. Tel.: +61 262 499 381; fax: +61 262 499 972.
E-mail address: Barry.Drummond@ga.gov.au (B.J. Drummond).

0040-1951/$ - see front matter.
doi:10.1016/j.tecto.2004.07.040

contrasts using real data. The highest amplitude reflections are likely to yield overestimates of the true impedance contrast.

Keywords: Seismic; Out-of-plane energy; Amplitudes; Imaging

1. Introduction

Reviews of deep seismic reflections suggest a number of sources for the reflections. They include lithological layering within rocks that are otherwise broadly uniform; sills emplaced into rocks of different composition or metamorphic grade; shear zones, in which the reflectivity could come from juxtaposing rocks of different type, or from chemical alteration and anisotropy within and adjacent to the shear zone; and from fluids deep in the crust (e.g., Matthews and Cheadle, 1986; Klemperer et al., 1987; Jones and Nur, 1982, 1984; Etheridge and Vernon, 1983).

The interpretation of deep crustal reflections usually remains ambiguous. Exceptions occur when the rocks being imaged extend up dip and crop out (e.g., Goleby et al., 1989) or are penetrated in a deep drill hole (Ganchin et al., 1998). In some cases, the ambiguity can be reduced, for example, where geometric relations between bundles of reflections suggest an interpretation consistent with other geological information; e.g., the detection of a regional detachment in the upper crust of the Yilgarn Block in Western Australia (Swager et al., 1997). Some studies attempted to reduce the ambiguity through quantitative analysis of the amplitude and phase of the reflections; e.g., interpretation of mafic dykes in the crust by Mandler and Clowes (1998). However, even when consensus is reached on the underlying cause of the reflections, there can remain debate on details. For example, Brown et al. (1996) suggested that fluids interpreted in the crust in Tibet are magmas, whereas Makovsky and Klemperer (1999) proposed that they are brines.

The ambiguity in interpreting deep crustal reflections that do not reach the surface and are not intersected in deep drill holes probably results in part from the apparently complex nature of the reflections. They often have a short lateral extent on stacked data and can therefore be difficult to migrate to their correct position. Unlike seismic images of sedimentary basins, they form complex geometric relationships that do not always suggest a causal geology. One of the major constraints in unambiguously interpreting deep crustal reflections is probably that reflections interpreted to be from some types of structures do not look like they have come from those types of structures. For example, reflections interpreted to be from fault zones are often not single reflections as would be expected from a plane between two pieces of rock, but rather are bands of reflections. Within the bands of reflections, individual reflections have variable and often limited lateral extent, although the bands themselves are more continuous. Similarly, the reflections interpreted to be sills by Mandler and Clowes (1998) were often bands or groups of reflections, rather than resembling in detail the pattern of a swarm of sills. In many studies, the amplitudes of reflections that are recorded are at the extreme range or exceed those expected when realistic physical properties are assumed for the geological models.

Deep seismic reflection studies almost invariably rely of single profiles, or at best multiple profiles separated by distances greater than the scale lengths of the structures being studied. The acquisition and data processing stages of the studies therefore have an underlying assumption that the structures are two-dimensional (2D). In an earlier study (Hobbs et al., submitted for publication), we showed that synthetic seismograms calculated along a profile across a three-dimensional structure, and processed as if the data were from a 2D structure, were different in shape to the 3D structure. This is because in a 3D model, out-of-plane seismic energy can enter the plane of the section, and in-plane energy can be reflected from the plane.

In this paper, we briefly review our previous work to reinforce the finding that collecting and processing deep seismic data assuming that the structures are 2D contributes to the complex form of deep seismic reflections, and can lead to ambiguity in how to interpret the reflections. That review then forms the basis of a qualitative analysis of the effects out-of-plane

energy on the amplitudes of seismic reflections. We show that using the strongest reflections in the section can lead to an overestimate of impedance contrast.

2. Reflections in three-dimensional media

2.1. Example of reflections from a complex layer

In our previous study, we considered the nature of reflections from shear zones using as an example a detachment in the upper crust of the Archaean Yilgarn Block of Western Australia. The detachment had been interpreted by Swager et al. (1997) as a horizontal shear zone or décollement based on geometrical relationships between the reflections and the overlying sequences. Subsequently, the detachment was imaged in a broad network of regional seismic profiles (Goleby et al., 2002). The reflections form a band that is continuous over 100 km laterally, although its character varies from place to place. One portion of the detachment used in our study is shown in Fig. 1(a). We

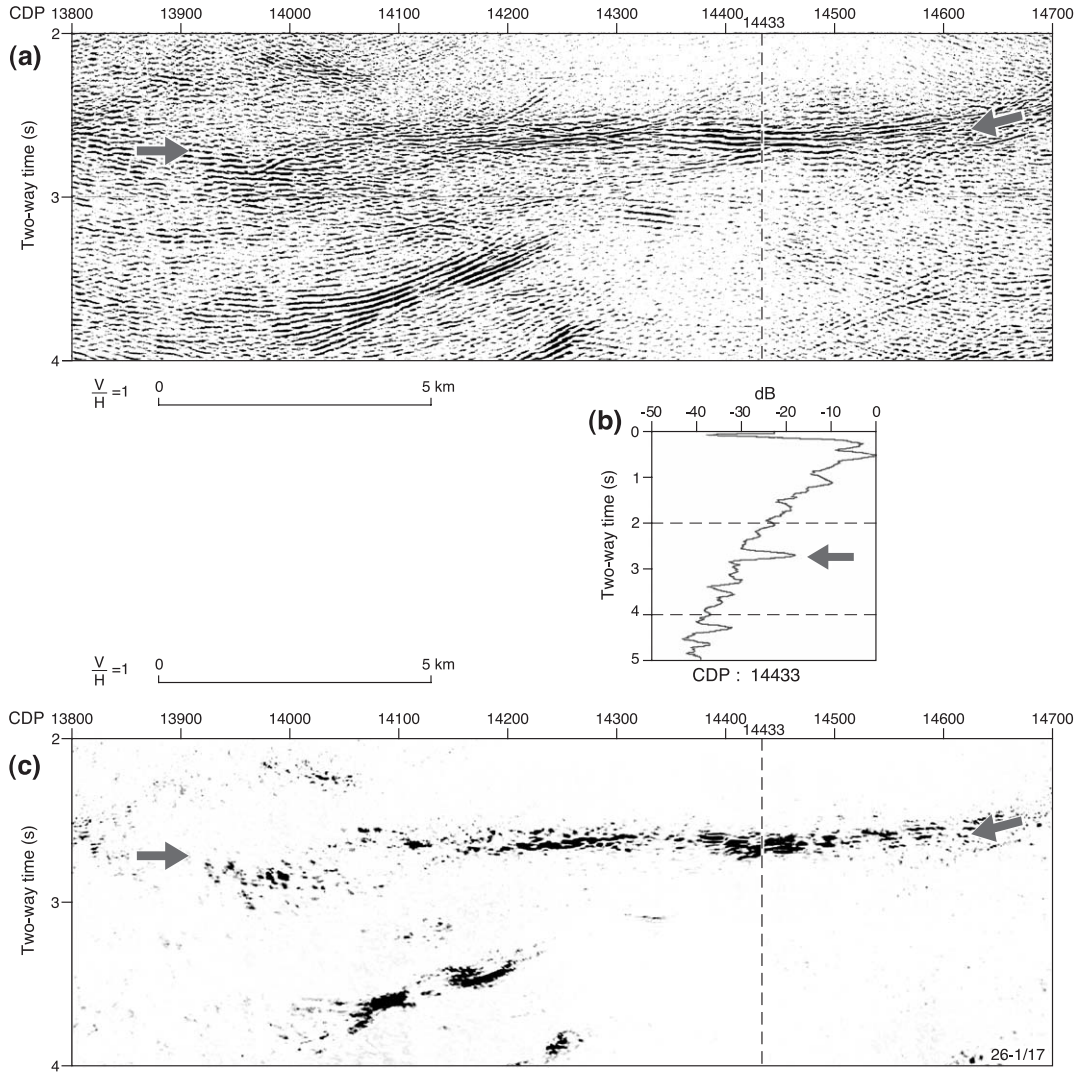

Fig. 1. Example of a sub-horizontal detachment, or décollement. (a) Post-stack migrated data. (b) Amplitude decay curve through the crust for a single unprocessed trace at an offset of 960 m that contributed to the gather for CDP 14433. Arrow shows the spike associated with the strong reflections from the Detachment. (c) Energy section. Arrows mark either end of the detachment in parts (a) and (c) of this figure.

chose it because gravity modelling using the geometries of rock bodies interpreted from the seismic data had indicated that the rocks above and below the detachment in this area probably have the same density. When combined with estimates of seismic velocity, the rocks above and below the detachment are likely to have similar seismic impedance, and the reflections would be caused by intrinsic reflectivity within the shear zone rather than the juxtaposition of rocks of different impedance.

The detachment lies between the arrows in Fig. 1(a), and has an apparent thickness of approximately 1 km, measured in the seismic time section as approximately 300 ms two-way-time (TWT). In the region between the arrows, the detachment is sub-horizontal. The top of the band of reflections has limited topography of 150–300 m (50–100 ms TWT). At the right hand end of the figure, it curves upward to a shallower depth to the right of the figure. At the left hand, it has smaller amplitude reflections and they are more diffuse.

The detachment is remarkable in the seismic section because of its very high amplitude reflections. The highest amplitude reflections occur in the common depth point (CDP) range 14,400–14,500. Fig. 1(b) shows the decay curve for the amplitude envelope of a single trace at 960 m offset in an unprocessed shot gather. The trace falls at CDP 14433. The amplitude envelope was calculated by taking the Hilbert Transform of the trace. The decay curve shows a spike approximately 10 db above the background decay curve at 2.6 s, close to the top of the band of reflections that define the detachment. Fig. 1(c) is a plot of energy in the same window as Fig. 1(a). It was generated by calculating the square of the amplitude envelope. In the CDP range 14,400–14,500, energy levels are generally higher than those to the left and right of that CDP range, and much higher than the background energy level above and below the detachment.

2.2. The shape of reflections

The seismic section in Fig. 1(a) was recorded as a single 10-fold profile. Data were sorted, stacked and migrated assuming that all data were from within the plane of the section. The detachment in Fig. 1(a) has a small amount of topography. We have no reason to assume that the topography is two-dimensional; i.e., the detachment may have comparable or even greater out-of-plane topography.

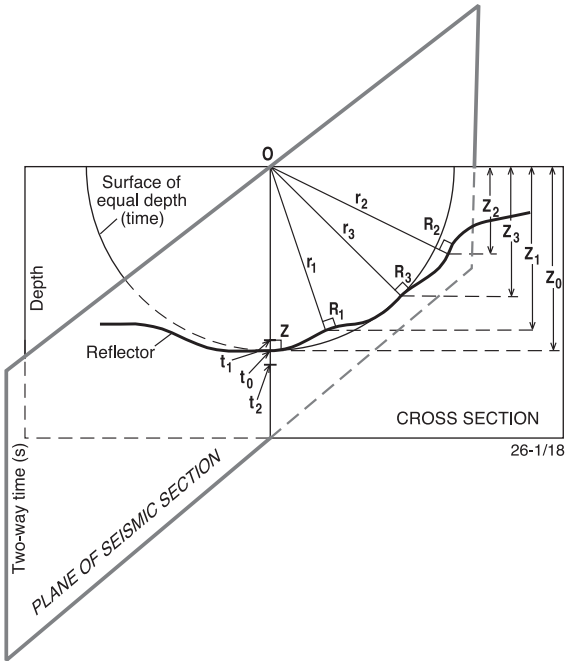

Fig. 2. Diagrammatic representation of the intersection of a reflector with a plane oriented at high angle to the plane of the seismic section.

The effects of out-of-plane topography on energy recorded along a seismic profile were considered in detail by Hobbs et al. (submitted for publication), and can be summarised using Fig. 2. It shows in diagrammatic form the intersection of the vertical plane of a seismic section with a cross-section in which a reflector has topography that slopes upwards to the right of the seismic section.

Note that the vertical axis on the seismic section is labelled in TWT, and in the cross-section it is labelled in depth. Making the simple assumption that the rocks above the reflector are isotropic and homogeneous, then TWT is proportional to depth, and for out-of-plane energy, proportional to the distance travelled by the seismic energy. For an observation point at O, in-plane seismic energy would come from the reflector Z, a distance z vertically below O, and will arrive at time t_0. The semi-circle with radius z_0 represents a surface of depth points with the same travel time. Energy reflected from parts of the surface that lie inside the semi-circle will arrive before the in plane reflection (e.g., $r_1<z_0$ so reflections from a reflection point R_1 will arrive at t_1, where $t_1<t_0$). Energy reflected from

parts of the surface that lie outside the semi-circle will arrive later than t_0 (e.g., those from R_2 will arrive at $t_2>t_0$ because $r_2>z_0$). Energy reflected from parts of the surface that lie on the semi-circle will arrive at the same time as the in-plane reflection (e.g., those from R_3 will arrive at t_0 because $r_3=z_0$). Therefore, out-of-plane topography can result in multiple reflections at different times from a single reflector. Cohen and Bleistein (1983) made a similar finding.

The reflection times t_1, t_2 and t_3 when converted to depth imply depths that are greater than z_1, z_2 and z_3, the depths of R_1, R_2 and R_3, respectively. For example, R_2 is quite high in the cross-section but plots low in the seismic section. Note also that R_2 is higher in the cross-section than R_1, but energy from R_2 will be recorded after that from R_1 in the seismic section. The position at which out-of-plane energy will be recorded is a function of both the topographic relief on the reflector and the offset of the relief from the plane of the section (Hobbs et al., submitted for publication).

The above discussion considers the behaviour of out-of-plane energy in a zero offset section; i.e., in stacked data. In single seismic profiles, the energy is then migrated in the plane of the section. A diffraction hyperbola for a point outside the plane of the seismic section, e.g., R_2, will be three-dimensional in form and will intersect the plane of the seismic section along a 2D hyperbolic curve with, in the case of R_2, its apex at t_2. Given our isotropic assumption, it will have the same moveout as a diffraction from a point reflector in the plane of the seismic section at the depth represented by t_2. The diffracted energy from R_2 will therefore migrate in the plane of the section as if the reflection point was at t_2 in the plane of the seismic section. This means that a coherent reflection from outside the plane of the seismic section will migrate in the plane of the seismic section to a depth that is greater than its real depth out of the plane of the section (Hobbs et al., submitted for publication), and different from the depth of the reflector in the plane of the section. Yilmaz (1987, p. 385) noted that this effect causes misties around loops in 2D seismic data in the exploration industry.

We illustrate these points in Figs. 3–5. Fig. 3 shows a surface generated using a double Fourier series to contain dominant wavelengths of 4.2 km in the direction of the arrows and 5.1 km at right angles. These are approximately representative of the longer wavelengths observed in the detachment surface in

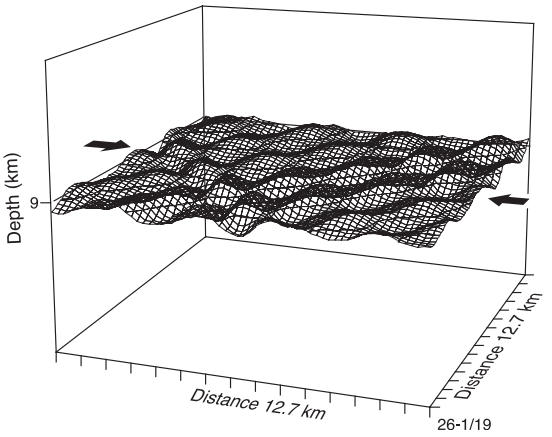

Fig. 3. Surface used to build the geological models in Figs. 4(a) and 5(a). Based in Fig. 4 of Hobbs et al. (submitted for publication). Arrows mark the line of the sections in Figs. 4 and 5.

Fig. 1. Smaller wavelengths were added to the surface, containing random phase shifts, and amplitudes that decreased at smaller wavelengths, to give the surface a component of randomness. The maximum peak to trough topographic relief on the surface was scaled to 250 m, approximately that of the top of the bands of reflections from the detachment in Fig. 1(a). A reflection layer 50 m thick was then generated bounded top and bottom by identical surfaces, and centred at a 9-km depth (equivalent to 2.8 s TWT), approximately the depth of the regional detachment in Fig. 1. The velocity was set to 6.5 km s^{-1} in the layer, and 6.4 km s^{-1} in the rocks above and below the layer.

A similar thickness horizontal layer also with a velocity of 6.5 km s^{-1} was placed at 7.92-km depth to provide a reference reflection. All synthetic seismic sections were processed so that the amplitudes of the reference layer were the same, so that the amplitudes of reflections from the deeper reflector surface could be compared from section to section.

The phase screen method of Wild and Hudson (1998) and Wild et al. (2000) was used to calculate two sets of synthetic seismograms along a cross-section whose position is marked by arrows in Fig. 3. Tests had shown that an exploding reflector approach was faster than and gave comparable results to generating and then stacking individual shot gathers along a multi-fold common mid-point profile. The source was a Ricker wavelet with a dominant frequency of 50 Hz. The stack data were Stolt migrated at the background velocity of 6.4 km s^{-1}.

The cross-section of the surface in the plane of the seismic section is shown in Fig. 4(a). The first set of synthetic seismograms assumed that the reflector layer did not have any out-of-plane topography; i.e., it was 2D. The post-stack migrated synthetic seismograms for the 2D model are shown in Fig. 4(b). Note that in this and subsequent sections, 505 traces were calculated at a spacing of 25 m to ensure accurate migration, but only every fifth trace is shown to ensure clarity in the diagram. The second set of synthetic seismograms was calculated for the reflector layer with out-of-plane topographic relief, as in Fig. 3; i.e., it was 3D. Fig. 4(b) provides a reference against which Fig. 4(c) can be assessed, because Fig. 4(b) represents the in-plane energy generated along the seismic line, whereas in Fig. 4(c), in-plane energy is lost from the section, and out-of-plane energy enters the section and combines with the remaining in-plane energy.

The data are presented with limited gain and no clipping so that they show the correct relative amplitudes. This highlights the variations in amplitudes across each section and relative to the reference reflections. In each of Fig. 4(b and c), the reflector layer is centred on about 2.8 s TWT, and the reference layer is at 2.5 s TWT. In general, the amplitudes in the synthetic data are reliable except at the edges of the model where absorbing boundaries attenuate the wavefield to minimise modelling artefacts and for parts of the reflector with steeper dips where energy is lost because it is scattered outside the edges of the model. This effect can be seen for the left most sinusoid in Fig. 4(b).

The differences between the seismograms in Fig. 4(b and c) illustrate the effects of out-of-plane energy on the seismic section. The travel times of reflections in the 2D model in Fig. 4(b) accurately reproduce the reflector topography if 2D processing and migration routines are used. In contrast, the geometry of the reflections from the reflector layer in Fig. 4(c) differs in several significant ways from the geometry of the layer. Firstly, below and for about 1.5 km to the right of the label “A”, two reflections and not one are recorded. At this point, in-plane energy impacting on the reflector in the vertical plane of the seismic section is reflected out of the plane of the section. The first arrival is from slightly out of the plane. The second arrival is from an antiform farther from the plane of the section. Both out-of-plane reflections are coherent within the plane of the section. At “B”, the first arrival is from a topographic high out of the plane of the section, and the second arrival is from within the plane of the section. At “C”, the topographic relief out of the plane is less than at “B”, and both the in-plane and some out-of-plane energy arrive at the same time. This affects the amplitude of the reflections, which is discussed below.

From these results, we conclude that 3D structure on a reflector can result in several reflections. The top reflection may not be an accurate guide to the position of the reflector at depth in the plane of the seismic section, especially in regions with significant relief at short offsets from the plane of the section. Although these results come from a model in which a reflecting layer was used, rather than an interface between two different rock bodies, the results also apply to interfaces.

So far, we have considered single layer reflectors in the crust. Some features are multi-layered. Examples would be shear zones, in which layers of chemically altered and strained, anisotropic rock anastomose around and between blocks of protocrust, and rocks with a dominant fabric and direction of composition, such as gneisses. The Moho in some regions has been described in both geological and geophysical studies as a transition zone involving alternating layers of quartzo-feldspathic, mafic and ultramafic rocks (Griffin and O’Reilly, 1987; Wass and Hollis, 1983; Ferguson et al., 1979; Fuchs, 1969; Mosegaard et al., 1997).

The effects of multiple layers on reflection character are addressed in Fig. 5. Fig. 5(a) is a cross-section through a model built with the layer discussed in Fig. 4 for single layer reflectors repeated eight times with different thicknesses, polarities, and

Fig. 4. (a) Cross-section of a single layer. (b) Synthetic seismogram for a 2D layer. Reference reflection is at the top. (c) Synthetic seismogram for 3D layer. Single asterisk marks trace with the largest amplitude. (d) Energy section for the synthetic data in (b). (e) Energy section for the synthetic data in (c). Single asterisk marks trace with the largest energy. (f) Difference between the energy section in (e) and the energy section in (d). Black filled areas indicate net energy gain to the plane of the section; white filled areas indicate net energy loss. Single asterisk marks greatest net energy loss from plane of section for the 3D model; double asterisk marks greatest net energy gain. All synthetic data have been post-stack migrated.

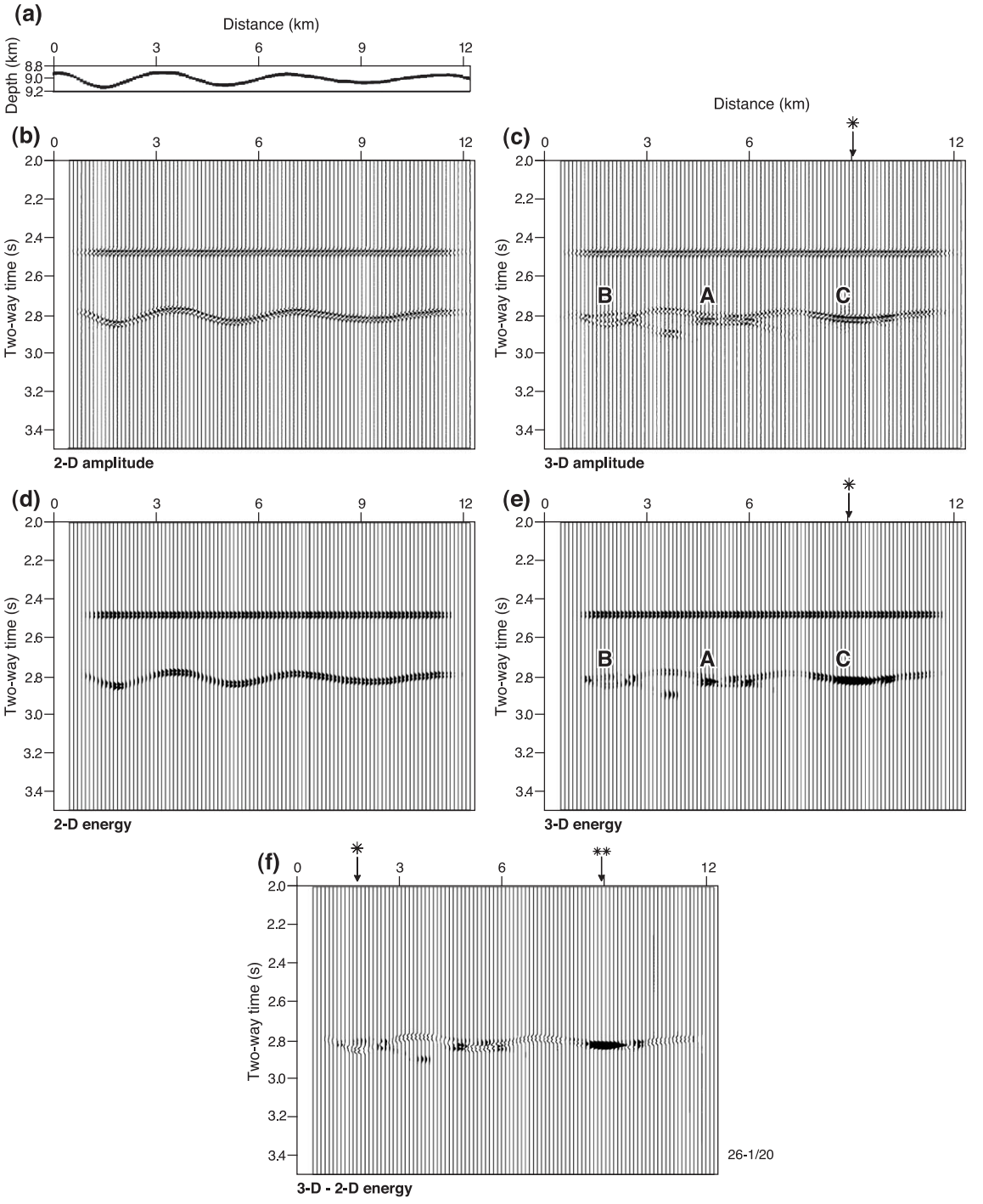
(a)
Distance (km)
0
3
6
9
12
Depth (km)
8.8
9.0
9.2
(b)
(c)
Distance (km)
Two-way time (s)
2.0
2.2
2.4
2.6
2.8
3.0
3.2
3.4
B
A
C
2-D amplitude
3-D amplitude
(d)
(e)
2-D energy
3-D energy
(f)
3-D - 2-D energy
26-1/20

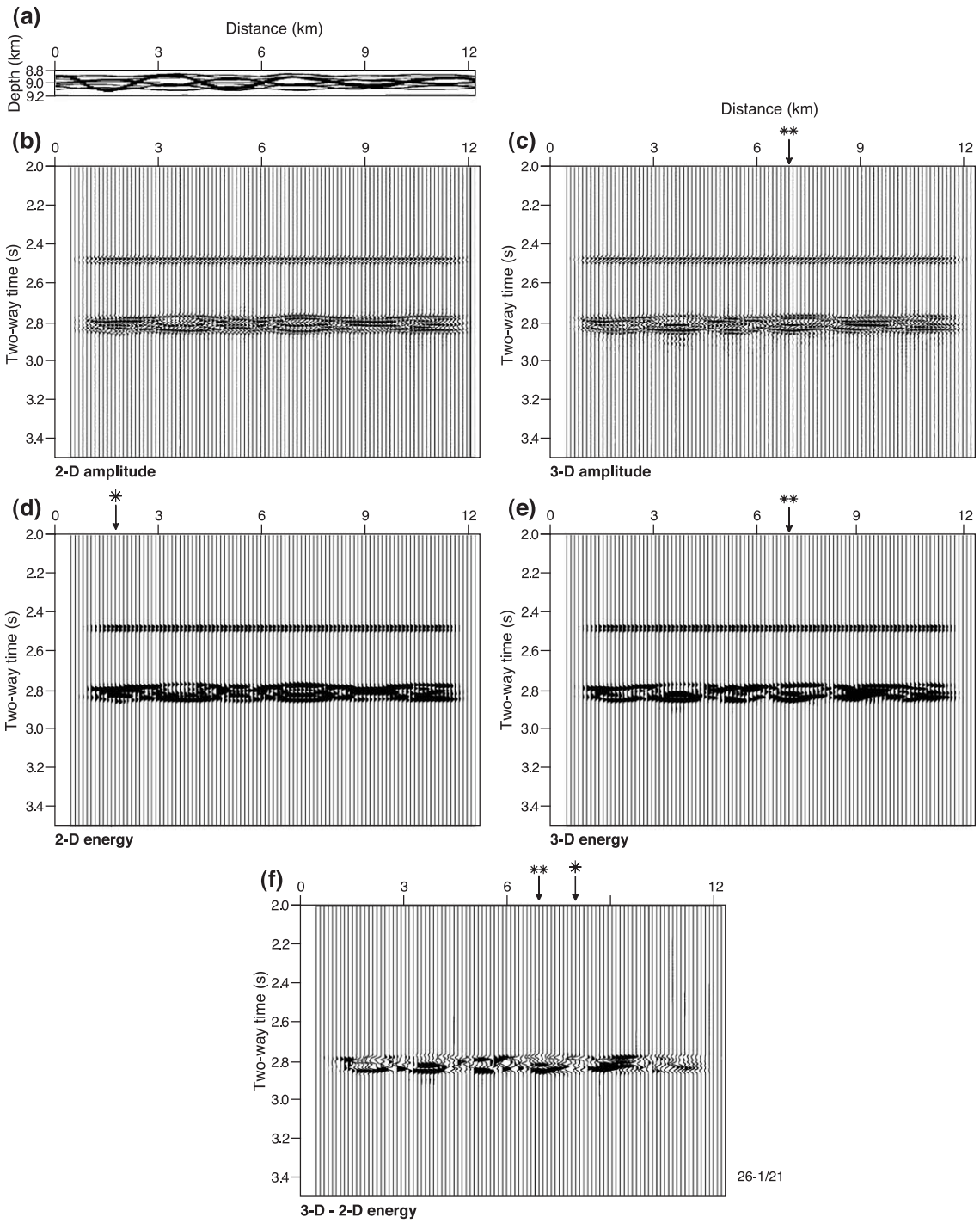
(a)
Distance (km)
Depth (km)
0
3
6
9
12
8.8
9.0
9.2
(b)
(c)
Distance (km)
Two-way time (s)
2.0
2.2
2.4
2.6
2.8
3.0
3.2
3.4
2-D amplitude
3-D amplitude
(d)
(e)
2-D energy
3-D energy
(f)
3-D - 2-D energy
26-1/21

moved in- and out-of-the plane of the seismic section so that the layer geometries have no correlation in space. Fig. 5(b) shows post-stack migrated synthetic seismograms for a 2D model in which the structure is assumed to have no out-of-plane topographic relief, and Fig. 5(c) is the synthetic data for a 3D model. Both sections have a reference reflection at the top. The difference between the two synthetic seismograms illustrates the effects of out-of-plane structure on the seismic image.

A major feature of these sections is that the bands of reflections that constitute the images of the reflection zones consist of many short reflections. They are less continuous than those in Fig. 4(c). The short lateral length and number of reflections are diagnostic of multi-layered reflectors (Hobbs et al., submitted for publication).

The 2D section in Fig. 5(b) maps accurately in TWT the geometry of the top and bottom of the zone of reflectors. The 3D section in Fig. 5(c) maps the geometries less precisely. The position of the top of the reflection band is less affected by out-of-plane energy than the single layer in Fig. 4 because the multi-layer model in Fig. 5 has less topographic relief on the top of the envelope of reflectors than the single layer. The bottom of the reflection band from the 3D model is less distinct than that from the 2D model because the multiple 3D layers produce numerous in- and out-of-plane diffractions that interfere and migrate poorly. In real data with realistic levels of noise, it might be difficult to distinguish between migrated images such as those in Fig. 5(b and c), although Hobbs et al. (submitted for publication) suggested that the number of diffractions in stacked data and the indistinct bottom after migration in 3D cases might help distinguish between 2D and 3D multi-layered structure.

2.3. The amplitudes of reflections

In Fig. 2, we demonstrated that the differences between the times of arrival of out-of-plane energy t_1 and t_2 and in-plane energy t_0 depend on both the amplitude of the topographic relief and the offset of the relief from the plane of the section; i.e., it depends on the differences in distance between OR_1, OR_2, OR_3 and z_0, the radius of the semi-circle. Where the differences are large, several reflections can be recorded from a single reflector; where they are smaller, destructive and constructive interference can lead to reflections that range in amplitude from very small to several times the amplitude expected of a primary reflection.

To study the amplitudes of reflections in the synthetic seismograms, a further model (not shown in the figures) was constructed in which a horizontal reflecting layer was placed at 9-km depth, the average depth of the reflectors in models shown in Figs. 4 and 5. This gave a reference reflection with the same amount of amplitude attenuation as for the models in Figs. 4 and 5, but without the effects of reflector topography. In Fig. 4(b), the amplitudes of the reflection from the reflector layer are the same as those from the horizontal reflector model, except at the edges and regions of steep dip as explained earlier. This is because the 2D assumptions that underlie the generation and processing of the data are appropriate for the 2D structure. In Fig. 4(c), the amplitudes are different from those of the horizontal reflector model, and from those in Fig. 4(b). This is because the synthetic seismogram section is a 2D image of a 3D structure, and the 2D assumptions inherent in the processing of the data are inappropriate for the 3D structure.

In Fig. 4, (d) and (e) are energy sections of the synthetic data in (b) and (c), respectively. Fig. 4(f) shows the energy from Fig. 4(d) subtracted from the energy in Fig. 4(e). Fig. 4(f) demonstrates where net energy has entered the plane of the section from out-of-plane structure (filled black pulses) and net energy has been reflected from the plane of the section (white unfilled, or negative-going pulses).

At C (Fig. 4(c)), reflection amplitudes in the trace marked with an asterisk (*) are up to 2.6 times those

Fig. 5. (a) Cross-section of a shear zone containing 8 layers. (b) Synthetic seismogram for 2D zone. Reference reflection is at the top. (c) Synthetic seismogram for 3D zone. Asterisks mark trace with the largest amplitude. (d) Energy section for the synthetic data in (b). (e) Energy section for the synthetic data in (c). Asterisks mark trace with the largest energy. (f) Difference between the energy section in (e) and the energy section in (d). Black filled areas indicate net energy gain to the plane of the section; white filled areas indicate net energy loss from the plane of the section. Single asterisk marks greatest net energy loss from plane of section for the 3D model; double asterisk marks greatest net energy gain. Synthetic data have been post-stack migrated.

of the reference reflection from the horizontal layer. The energy (Fig. 4(e)) is higher in this region because net energy has come into the plane of the section from the reflector out of the plane of the section (Fig. 4(f)) and constructively interfered with the in-plane energy. Amplitudes and energy higher than the reference reflection occur below A, indicating that net energy has also come into the plane of the section in this region. However, about 700 m to the right of A, the amplitudes are less than the reference reflection. The energy from the two out-of-plane reflections that contributed to the higher amplitude arrivals below A arrived with a relative time delay sufficient for them to destructively interfere. A similar effect is seen at B. In summary, net energy has come into the plane of the section at each of the synforms, and whereas it has created large amplitude arrivals consistently at one synform (C), it has created both larger and smaller amplitude arrivals at the other two synforms (B and A). In contrast, over each of the antiforms in the surface, net energy has left the plane of the section. This is because the antiforms are oblique to the plane of the section and energy is reflected out of the plane of the section.

The multi-layer models in Fig. 5 demonstrate the effects of both vertical tuning and out-of-plane energy. Vertical tuning is demonstrated in Fig. 5(b), where no out-of-plane effects are possible. For wavelets with any reasonable bandwidth, anastomosing reflectors will be separated by lensoid and wedge-shaped areas where the thickness of the protolith somewhere in the model is likely to be tuned to the seismic wavelet. In this model, the maximum tuning occurs at the trace marked with an asterisk in Fig. 5(d), with trace amplitudes 2.05 times those of the reference reflector. This amplification is similar to that obtained by Spaargaren and Warner (1991) in their study of the maximum amplification likely to occur because of tuning caused by multiple layers. The first reflection has the largest amplitude. Many other reflections in this section have amplitudes greater than the reference reflection because of tuning.

In the seismic section for the multi-layer 3D model in Fig. 5(c), the largest amplitudes are 3.07 times those of the reference reflection, and occur in the last reflection on the trace marked with two asterisks. We cannot separate the effects of tuning and out-of-plane energy for this reflection, and assume that both effects are present. Tuning between layers in this case would also have to include out-of-plane energy, because the model was constructed in such a way that the layers cannot be parallel either in- and out-of-the section, or within the plane of the section. Fig. 5(f) highlights the small lateral distances over which amplitudes can change due to tuning and out-of-plane effects, with the largest net energy gain in the last reflection in the trace marked with two asterisks, and the greatest net energy loss nearby at the trace marked with one asterisk.

The net amount of out-of-plane energy gained or lost from the seismic section in Fig. 4(e) (single 3D reflecting layer) can be estimated by comparing its energy with that in Fig. 4(d). Fig. 4(e) has an approximate 15% energy gain. The section in Fig. 4(c) has a net energy gain because the synforms, and particularly the synform at the right hand end, have focussed out-of-plane energy into the section in a way that allows constructive interference with the in-plane energy. Energy was lost from the sections over the antiforms. Summed across a number of sections through the model, the amount of energy entering the sections and the amount of energy leaving the sections will balance, because no net energy can be created by slicing a three-dimensional seismic image into a number of two-dimensional sections. By analogy, if any section is sufficiently long and representative of structure of the model, it should show no net energy gain or loss. We therefore conclude that the section in Fig. 4 is not sufficiently long to be representative of the structures across the entire 3D single layer model, and that other sections through the model would show net energy losses.

The section in Fig. 5(c) for multiple 3D layers has no net gain or loss of out-of-plane energy. The multiple surfaces provide many more antiformal and synformal features than a single layer, increasing the likelihood that energy gains in synforms are compensated by energy losses over antiforms.

3. Discussion

The large amplitudes of some crustal reflections have attracted comment (e.g., Fuchs, 1969; Spaargaren and Warner, 1991; Mooney and Meissner, 1992; Mosegaard et al., 1997). Finding realistic geological

explanations for many of the large amplitudes has been difficult. However, in the bulk of the published models, reflection strength was studied using 1D physical models. The effect of 2D and 3D structure on reflection strength was ignored.

The results presented here show that when 3D reflector topography is present, the largest amplitude reflections in a section are probably poor indicators of the reflection coefficient of the reflector. Amplitude gains of 2.6 were recorded due to the effects of out-of-plane energy for single layer reflectors. Tuning between multiple layers in a 2D model (Fig. 5(b)) generated amplitude gains of 2.05, and the combined effects of tuning between layers and constructive interference of out-of-plane and in-plane energy created amplitude gains of 3.07. We cannot resolve the relative effects of tuning and out-of-plane energy, and can conceive contrived models in which the maximum tuning effect of about 2 could be made coincident with the maximum out-of-plane effects to give much greater amplitude gains. Synformal shaped reflectors will lead to high amplitudes and an over estimate of reflection coefficient. Reflection strength in antiformal structures will probably provide estimates of the impedance contrast that are too low. Unfortunately, in-plane structure may not be a good indicator of out-of-plane structure, and other a-priori information may be needed to assess out-of-plane structure and whether it may be affecting the recorded amplitudes. Multiple reflections from what might have been expected to be a single reflector would be one indication of out-of-plane topography on the reflector.

When multiple deep crustal reflections are recorded that are interpreted to have come from the same reflector (either a single reflector or a band of multiple reflectors), care must be taken when inferring the true position of the reflector or band of reflectors in the plane of the section. If the top reflection is an early out-of-plane reflection that has arrived before the in-plane energy (e.g., B in Fig. 4(c)), the true reflector position will be deeper than indicated. If in-plane energy is reflected out of the plane of the section, the first energy to arrive will be out-of-plane energy but in this case the true position of the reflector in the plane of the section will be shallower (e.g., A in Fig. 4(c)). These effects are more marked when the topographic relief out of the plane of the section is greatest.

The amplitudes of reflections are also a poor guide to the true position of the reflector. The highest amplitudes will occur where tuning and constructive interference between in- and out-of-plane energy occurs, and this can occur anywhere between the first and last reflections in a reflection band. In the single 3D layer model in Fig. 4(c), the large amplitudes near A are not the first arrivals. In the multi-layer 3D model in Fig. 5(c), the largest amplitudes are at the bottom of the reflection band.

To fully recover both correct amplitudes and travel times, the data must be migrated in 3D. Migration in 3D can be resolved into migration along the seismic line and migration at right angles to the seismic line (Yilmaz, 1987, p. 385). 2D surveys do not have sufficient data for out-of-plane migration. No amount of processing and manipulation of the data in 2D will resolve these problems. The use of quantitative analyses of reflection travel times, amplitudes and waveforms to reduce ambiguity in the interpretations of deep seismic reflection sections should therefore be done with caution, particularly when 1D physical models are used to explain features in 2D seismic sections recorded across 3D structures.

In this paper, we have assumed a simple homogeneous isotropic velocity model. This is valid for areas like the Yilgarn Block in Australia, where basement rocks crop out at the surface. In areas with sedimentary cover, velocity generally increases with depth. In such cases, our simple wavefront, in Fig. 2, ceases to be a hemisphere but the principle of out-of-plane contamination described in this paper will still be valid.

Acknowledgements

Angie Jaensch drew the figures. BJD and BRG published this work with the permission of the Chief Executive Officer of Geoscience Australia.

References

Brown, L.D., Zhao, W., Nelson, K.D., Hauck, M., Alsdorf, D., Ross, A., Cogan, M., Clark, M., Liu, X., Che, J., 1996. Bright spots, structure, and magmatism in Southern Tibet from INDEPTH seismic reflection profiling. Science 274, 1688–1690.

Cohen, J.C., Bleistein, N., 1983. The influence of out-of-plane surface properties on unmigrated seismic sections. Geophysics 48, 125–132.

Etheridge, M.A., Vernon, R.H., 1983. Seismic velocity and anisotropy in mylonites and the reflectivity of deep crustal fault zones; discussion. Geology 11, 487–489.

Ferguson, J., Arculus, R.J., Joyce, J., 1979. Kimberlite and kimberlitic intrusives of southeastern Australia: a review. BMR J. Aust. Geol. Geophys. 4, 227–241.

Fuchs, K., 1969. On the properties of deep crustal reflectors. Z. Geophys. 35, 133–149.

Ganchin, Y.V., Smithson, S.B., Morozov, I.B., Smythe, D.K., Garipov, V.Z., Karev, N.A., Kristofferson, Y., 1998. Seismic studies around the Kola Superdeep Borehole, Russia. Tectonophysics 288, 1–16.

Goleby, B.R., Shaw, R.D., Wright, C., Kennett, B.L.N., Lambeck, K., 1989. Geophysical evidence for 'thick-skinned' crustal deformation in central Australia. Nature 337, 325–330.

Goleby, B.R., Korsch, R.J., Fomin, T., Bell, B., Nicoll, M.G., Drummond, B.J., Owen, A.J., 2002. Preliminary 3-D geological model of the Kalgoorlie region, Yilgarn Craton, Western Australia, based on deep seismic-reflection and potential-field data. Aust. J. Earth Sci. 49, 917–933.

Griffin, W.L., O'Reilly, S.Y., 1987. The composition of the lower crust and the nature of the continental Moho. In: Nixon, P.H. (Ed.), Mantle Xenoliths. Wiley, London, pp. 413–430.

Hobbs, R.W., Drummond, B.J., Goleby, B.R., 2005. The effects of three dimensional shear zone morphology on the nature of reflections in two dimensional crustal seismic sections. Geophys. J. Int. (submitted for publication).

Jones, T.D., Nur, A., 1982. Seismic velocity and anisotropy in mylonites and the reflectivity of deep crustal fault zones. Geology 10, 260–263.

Jones, T.D., Nur, A., 1984. The nature of seismic reflections from deep crustal fault zones. J. Geophys. Res. 89, 3153–3171.

Klemperer, S.L., and the BIRPS Group, 1987. Reflectivity of the crystalline crust: hypotheses and tests. Geophys. J. R. Astron. Soc. 89, 217–222.

Makovsky, Y., Klemperer, S.L., 1999. Measuring the seismic properties of Tibetan bright spots: evidence for free aqueous fluids in the Tibetan middle crust. J. Geophys. Res. 104, 10795–10825.

Mandler, H.A.F., Clowes, R.M., 1998. The HIS reflector: further evidence for extensive magmatism in the Precambrian of western Canada. Tectonophysics 288, 71–81.

Matthews, D.H., Cheadle, M.J., 1986. Deep reflections from the Caledonides and Variscides west of Britain and comparison with the Himalayas. In: Barazangi, M., Brown, L. (Eds.), Reflection Seismology: A Global Perspective. AGU, Geodynamics Series, vol. 13, pp. 5–19.

Mooney, W.D., Meissner, R., 1992. Multi-genetic origin of crustal reflectivity: a review of seismic reflection profiling of the continental lower crust and Moho. In: Fountain, D.M., Arculus, R., Kay, R.W. (Eds.), Continental Lower Crust. Developments in Geotectonics, vol. 23, pp. 45–79.

Mosegaard, K., Singh, S.C., Snyder, D.B., Wagner, H., 1997. Monte Carlo analysis of seismic reflections from the Moho and the W-reflector. J. Geophys. Res. 102, 2983–2997.

Spaargaren, B., Warner, M., 1991. Constructive interference—geophysical mythology re-examined. In: Meissner, R., Brown, L., Dürbaum, H.-J., Franke, W., Fuchs, K., Seifert, F. (Eds.), Continental Lithosphere: Deep Seismic Reflections. AGU, Geodynamics Series, vol. 22, pp. 359–362.

Swager, C.P., Goleby, B.R., Drummond, B.J., Rattenbury, M.S., Williams, P.R., 1997. Crustal structure of granite–greenstone terranes in the Eastern Goldfields, Yilgarn Craton, as revealed by seismic reflection profiling. Precambrian Res. 83 (1–3), 43–56.

Wass, S.Y., Hollis, J.D., 1983. Crustal growth in south-eastern Australia—evidence from lower crustal ecologitic and granulitic xenoliths. J. Metamorph. Geol. 1, 25–45.

Wild, A.J., Hudson, J.A., 1998. A geometrical approach to the elastic complex screen. J. Geophys. Res. 103, 707–725.

Wild, A.J., Hobbs, R.W., Frenje, L., 2000. Modelling complex media: an introduction to the phase-screen method. Phys. Earth Planet. Inter. 120, 219–225.

Yilmaz, Ö., 1987. Seismic data processing. Soc. Explor. Geophys., Investig. Geophys. 2 (526 pp).